Full Paper Transactions, SMiRT 28
Toronto, Canada, August 10-15, 2025

OVERCOMING RCC-M CODE CONSERVATISMS FOR DESIGN OF CORNER-BOLTED STEEL-TO-CONCRETE END-PLATE CONNECTIONS

Maël SONNA DONKO[1], Maël COUCHAUX[2], Jean-Pierre BOUDOT[3]

[1] Research Engineer, PhD Candidate, Framatome, Lyon, France (mael.sonna-donko@framatome.com)
[2] Associate Professor, INSA Rennes, Rennes, France (mael.couchaux@insa-rennes.fr)
[3] Dr., Expert Engineer, Framatome, Lyon, France (jean-pierre-boudot@framatome.com)

ABSTRACT

The RCC-M code, particularly Volume H, provides a comprehensive set of design and construction rules for mechanical equipment in PWR nuclear islands, with a focus on the design and maintenance of supports for piping systems. While it does not directly address the anchorage of supports to concrete wall systems or steel-to-concrete end-plate connections, the guidelines it offers are based on elastic methods which, although conservative, are no longer fully aligned with the current state of the art. This conservative approach, particularly regarding steel-to-concrete end-plate connections, overlooks elastoplastic behaviour, focusing primarily on the elastic domain and using elastic criteria. In contrast, Eurocode 3 part 1-8 considers an elastoplastic behaviour, enabling significant gains in strength. As such, a movement is underway to transition towards the Eurocode philosophy while retaining the necessary margin for the nuclear industry. Despite this shift, the Eurocodes do not currently address the specific configurations of corner-bolted steel-to-concrete end-plate connections prevalent in the nuclear sector. This study presents an analytical model, based on the limit analysis, developed to determine the uniaxial and biaxial bending moment resistances of steel-concrete bolted end-plate connections with corner bolts. The proposed model is confronted to experimental tests performed by the authors on 12 connections and a good accuracy is obtained. The methods of RCC-M and AISC DG1 appear overconservative. The proposed method permits the computation of more realistic bending resistances of steel-to-concrete end-plate connections.

INTRODUCTION

The RCC-M code was established in 1981 to address the unique requirements of the French nuclear industry, which previously relied on the ASME Boiler and Pressure Vessel Code (1963) and revisions. Over the years, RCC-M evolved independently, introducing modifications to align with French standards. Focusing on supports, RCC-M's 2024 volume H (2025) reliance on conservative elastic methods often leads to underestimations of the strength of steel-to-concrete connections, particularly due to the systematic use of Lescouarc'h (1988) design approach and Delesques' (1971) effective lengths. During the last years, the French nuclear sector tends to adopt Eurocode design philosophies to integrate advanced elastoplastic design methods. However, Eurocode 3 part 1-8 assumes anchor bolts positioned within the flange width, contrasting with the nuclear sector's practice of placing bolts at the corners of end-plates. This discrepancy leaves a gap in explicit design methods for corner-bolted steel-to-concrete end-plate connections both in the RCC-M 2024 (2025) and Eurocode 3 (2005). While AISC DG1 (2024) address such configurations, they are deemed overly conservative, especially for thin end-plates. To address these gaps, this study proposes an analytical method based on limit analysis to evaluate the resistance of corner-bolted steel-to-concrete connections under in-plane, out-of-plane, and biaxial bending moments. The method adapts the Eurocode's T-stub approach to varying-width stubs, accommodating anchor bolt positions used in the nuclear industry. Validated through 12 experimental tests results performed by the authors (2025), the method demonstrates greater accuracy than current RCC-M and AISC DG1 methods, which were found to be overly conservative. The proposed method offers a more precise assessment by incorporating detailed

representations of anchor bolt force redistributions and contact pressures, closely aligning with experimental results.

VARYING-WIDTH HALF T-STUB

The proposed design method is based on extensive experimental observations and numerical analyses conducted by the authors to accurately assess the resistance of steel-to-concrete end-plate connections under various bending conditions. The component method of Eurocode 3 Part 1-8 (2005) is used dividing the connection into tensile and compressive areas. The tensile area is modelled considering half T-stubs with varying width (see Figure 1).

a) b)

Figure 1. T-stub models a) Eurocode 3 Part 1-8 (EN 1993-1-8) conventional T-stub configuration b) Half T-stub with varying width

MODEL ASSUMPTIONS

The proposed model is based on several key assumptions, combining both established and experimental-based novel perspectives to accurately assess the behaviour of steel-to-concrete end-plate connections. One fundamental assumption is that the section of the end-plate beneath the beam remains rigid. This is justified by the high in-plane stiffness of the flanges and web, ensuring the end-plate stays flat.

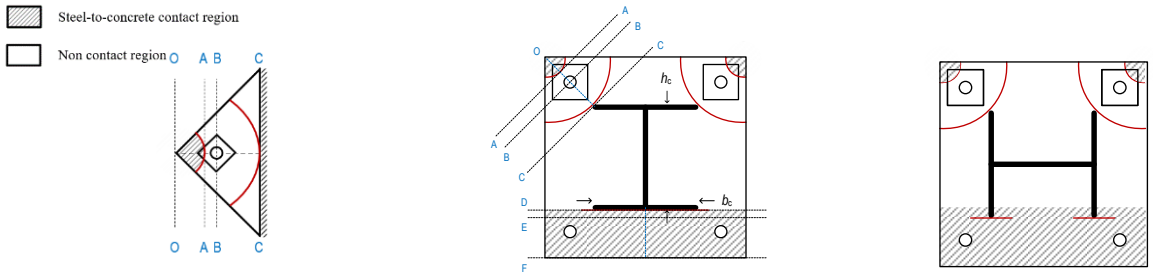

a) b) c)

Figure 2. Yield lines in the end-plate a) Varying-width end-plate section *OC* b) In-plane bending c) Out-of-plane bending

In the tensile area, the end-plate is treated as a varying-width half T-stub that extends from the flange edge, passes through the anchor bolt centre, and reaches the end-plate corner (*OC*) as seen in Figure 2a. In contrast, in the compressive area, the end-plate is modelled as a uniform-width L-stub extending from the flange in compression to the edge of the end-plate (*DF*).

The model includes experimentally observed yield lines in both tension and compression zones of the end-plate (see Figure 2). In the tensile zone, yield lines are assumed circular from the flange tip to the end-plate corner through the anchor bolt, accommodating both square and rectangular plates. Kanvinde et al. (2015) and Fasae et al. (2018) highlighted the presence of circular yield lines in corner-bolted connections (see Figure 3-a and b). In the compressed part, linear yield lines observed by Sonna Donko et al. (2024, 2025) are considered (see Figure 3-c).

a) b) c)

Figure 3. Experimental observations of yield lines a) Kanvinde et al. (2015) b) Fasae et al. (2018) c) Sonna Donko et al. (2024)

Based on experimental findings, portrayed in Figure 3c, showing that yield lines typically form between the anchor bolt axis and the end-plate corner, the model introduces a new failure mode involving double curvature bending of the end-plate and anchor bolt failure in tension. Additionally, EN 1993-1-8's failure Mode 2 is refined by incorporating the distributed surface area of prying forces at the end-plate corners (highlighted white region on Figure 3c).

A rigid-plastic approach is employed for both the steel end-plate and concrete foundation. By ensuring equilibrium between the tensile and compressive forces, the method evaluates individual half T-stub resistances and integrates them to determine the overall bending resistance for uniaxial and biaxial bending moments. An elliptical interaction curve is used for biaxial bending moment.

In the following sections, analytical expressions for the resistance of tensile and compressive areas are proposed for both in-plane and out-of-plane bending moments.

RESISTANCE OF THE TENSILE AREA

The proposed approach for evaluating the resistance of the tensile area is based on EN 1993-1-8 method but introduces refined considerations for prying effects and a new failure mode. The applicable failure modes depend on the presence or absence of prying effects by evaluating anchor bolt elongation against EN 1993-1-8's threshold, L_b^* given by:

$$L_b^* = \frac{4.4 m_x^3 \cdot A_s}{l_{eff,1} t_p^3} \quad (1)$$

Where, t_p is the thickness of the end-plate, A_s, the anchor bolt's net cross-sectional area, m_x, its distance to the root of the weld and, $l_{eff,1}$, an effective length given in Table 1. The anchor bolt elongation length is calculated as the total of eight times the nominal bolt diameter, plus the grout layer (if applicable), plate thickness, washer, and half of the nut height. If this length is less than L_b^*, prying effects develop, and failure modes 1, 2-1, 2, and 3 are considered. Without prying effects, only failure modes 1-2 and 3 apply.

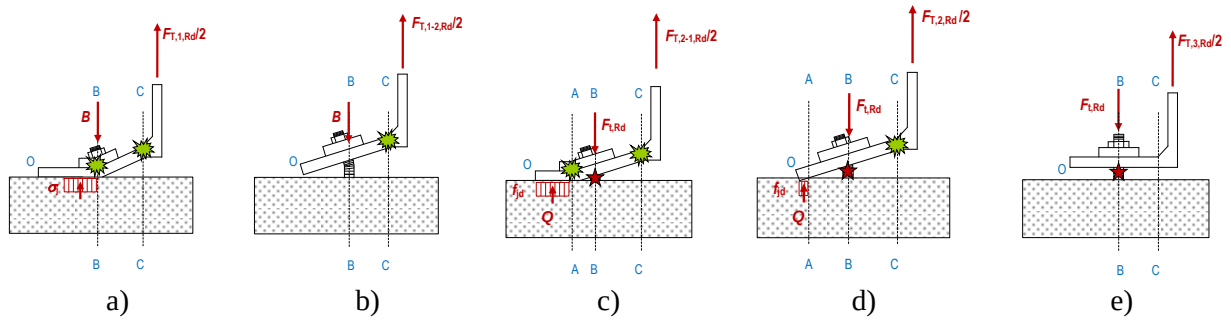

Figure 4. Failure modes of half T-stubs in tension a) Mode 1 b) Mode 1-2 c) Mode 2-1 d) Mode 2 e) Mode 3

Experimental findings highlight that the contact pressure distributions develop over a surface and is not positioned at the free edge. Additionally, a new failure mode (see Figure 4), labelled mode 2-1, was identified and was characterized by double curvature yielding of the end-plate and anchor bolt failure.

The half T-stub resistance corresponds to the minimum resistance obtained through direct application of the kinematic theorem, accounting for the various failure modes. The analysis includes a detailed examination of the separation length (*AA*-*BB*) to determine the extent of contact area. Additionally, the method extends EN 1993-1-8 by adapting mode 1 for varying width of the half T-stub, providing a more accurate assessment of corner-bolted configurations, while failure mode 3 remains unchanged.

Mode 2-1

In this failure mechanism, two yield lines develop in the end-plate, creating distinct rigid zones: segment *OA*, which remains in contact with concrete, and segment *ABC*, which lifts away. With this failure mode, the yield line does not pass directly through the anchor bolt but rather between the bolt and the corner of the end-plate (see Figure 5). This finding necessitates determining the optimal position for point *A* to minimize energy. The tensile resistance is obtained with principles of virtual work:

$$F_{\mathrm{T,2\text{-}1,Rd}} = \frac{2\left(M_{\mathrm{pl,A,Rd}} + M_{\mathrm{bp,A,Rd}} + M_{\mathrm{pl,C,Rd}}\right) + F_{\mathrm{t,Rd}} \dfrac{\left(d_{\mathrm{bp}} + 2\xi_{\mathrm{T,2\text{-}1}}\right)^2}{4d_{\mathrm{bp}}}}{m_{\mathrm{x}} + \xi_{\mathrm{T,2\text{-}1}}} \tag{2}$$

Where,

$$M_{\mathrm{pl,A,Rd}} = \frac{\pi\left(e_{\mathrm{x}} - \xi_{\mathrm{T,2\text{-}1}}\right)t_{\mathrm{p}}^2 f_{\mathrm{y}}}{8\gamma_{\mathrm{M0}}},\ M_{\mathrm{bp,A,Rd}} = \frac{\pi\left(d_{\mathrm{bp}} - 2\xi_{\mathrm{T,2\text{-}1}}\right)t_{\mathrm{bp}}^2 f_{\mathrm{y,bp}}}{16\gamma_{\mathrm{M0}}},\ M_{\mathrm{pl,C,Rd}} = \frac{\pi\left(m_{\mathrm{x}} + e_{\mathrm{x}}\right)t_{\mathrm{p}}^2 f_{\mathrm{y}}}{8\gamma_{\mathrm{M0}}} \text{ and } F_{\mathrm{t,Rd}} = \frac{0.9 f_{\mathrm{ub}} A_{\mathrm{s}}}{\gamma_{\mathrm{M2}}}$$

f_{y} and $f_{\mathrm{y,bp}}$ are the end-plate's and backing plates yield strength respectively, f_{ub}, the anchor bolt's ultimate tensile strength, $F_{\mathrm{t,Rd}}$, the anchor bolt tensile resistance and γ_{M2}, is the partial coefficient taken as 1.25.

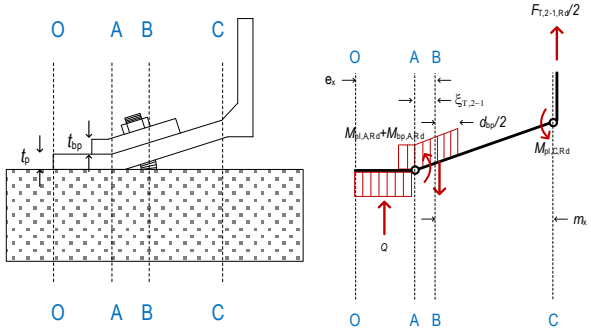

Figure 5. Mode 2-1, anchor bolt failure and complete end-plate yielding

$\xi_{T,2\text{-}1}$ is determined minimizing the energy:

$$\xi_{T,2\text{-}1} = -m_x + \sqrt{m_x^{\,2} + d_{bp}\left(\frac{\pi}{4F_{t,Rd}}\left(2(m_x + e_x)t_p^2\frac{f_y}{\gamma_{M0}} + \frac{1}{2}(2m_x + d_{bp})t_{bp}^2\frac{f_{y,bp}}{\gamma_{M0}}\right) - \left(m_x - \frac{d_{bp}}{4}\right)\right)} \tag{3}$$

When $\xi_{T,2\text{-}1} > d_{bp}/2$, the proposed failure mode is invalid.

Mode 2

Failure mode 2 corresponds to anchor bolt failure in tension with concrete crushing at the end-plate corner (OA) and the development of a yield line near the weld at point C (see Figure 6).

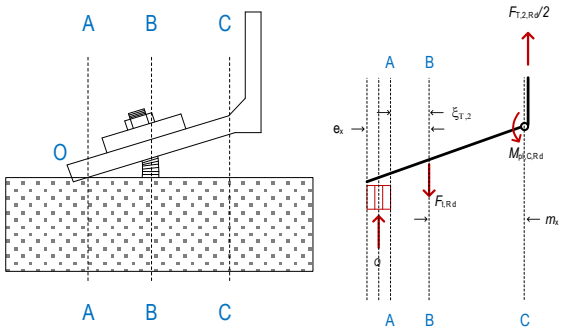

Figure 6. Mode 2: anchor bolt failure and end-plate yielding

The tensile resistance, $F_{T,2,Rd}$, as well as the separation length, $\xi_{T,2}$, are determined with equilibrium:

$$F_{T,2,Rd} = \frac{2M_{pl,C,Rd} + 2F_{t,Rd}\left(e_x + \xi_{T,2}/2\right)}{m_x + e_x + \xi_{T,2}/2} \tag{4}$$

With:

$M_{pl,C,Rd}$: Plastic bending moment:

$$M_{\mathrm{pl,C,Rd}} = \frac{\pi\left(m_{\mathrm{x}} + e_{\mathrm{x}}\right)t_{\mathrm{p}}^{2} f_{\mathrm{y}}}{8\gamma_{\mathrm{M0}}}$$

Table 1 : Resistance of equivalent T-stub in tension

<table>
<tr><td>Failure mode</td><td colspan="2">Presence of prying effect: $L_{\mathrm{b}} \le L_{\mathrm{b}}^{*}$</td><td>No prying effect: $L_{\mathrm{b}} > L_{\mathrm{b}}^{*}$</td></tr>
<tr><td>Mode 1: Complete end-plate yielding</td><td>Method 1</td><td>Method 2 (Alternative method)</td><td rowspan="4">$F_{\mathrm{T,1-2,Rd}} = \dfrac{2M_{\mathrm{pl,1-2,Rd}}}{m_{\mathrm{x}}}$</td></tr>
<tr><td>Without backing-plates</td><td>$F_{\mathrm{T,1,Rd}} = \dfrac{4M_{\mathrm{pl,1,Rd}}}{m_{\mathrm{x}}}$</td><td>$F_{\mathrm{T,1,Rd}} = \dfrac{\left(8n_{\mathrm{x,1}} - 4e_{\mathrm{w}}\right)M_{\mathrm{pl,1,Rd}} + 4e_{\mathrm{w}}M_{\mathrm{pl,1,A,Rd}}}{2m_{\mathrm{x}}n_{\mathrm{x,1}} - e_{\mathrm{w}}\left(m_{\mathrm{x}} + n_{\mathrm{x,1}}\right)}$</td></tr>
<tr><td>With backing plates</td><td>$F_{\mathrm{T,1,Rd}} = \dfrac{4M_{\mathrm{pl,1,Rd}} + 2M_{\mathrm{bp,1,Rd}}}{m_{\mathrm{x}}}$</td><td>$F_{\mathrm{T,1,Rd}} = \dfrac{\left(8n_{\mathrm{x,1}} - 4e_{\mathrm{w}}\right)M_{\mathrm{pl,1,Rd}} + 4e_{\mathrm{w}}M_{\mathrm{pl,1,A,Rd}} + 4n_{\mathrm{x,1}}M_{\mathrm{bp,1,Rd}}}{2m_{\mathrm{x}}n_{\mathrm{x,1}} - e_{\mathrm{w}}\left(m_{\mathrm{x}} + n_{\mathrm{x,1}}\right)}$</td></tr>
<tr><td>Mode 2-1: Complete end-plate yielding with anchor bolt failure</td><td colspan="2">$F_{\mathrm{T,2-1,Rd}} = \dfrac{2M_{\mathrm{pl,2-1,Rd}} + 2M_{\mathrm{bp,2-1,Rd}} + F_{\mathrm{t,Rd}}\left(2e_{\mathrm{bp}} + \xi_{\mathrm{T,2-1}}\right)^{2} \Big/ 4e_{\mathrm{bp}}}{m_{\mathrm{x}} + \xi_{\mathrm{T,2-1}}}$</td></tr>
<tr><td>Mode 2: Anchor bolt failure with end-plate yielding</td><td colspan="2">$F_{\mathrm{T,2,Rd}} = \dfrac{2M_{\mathrm{pl,2,Rd}} + 2F_{\mathrm{t,Rd}}n_{\mathrm{x,2}}}{m_{\mathrm{x}} + n_{\mathrm{x,2}}}$</td></tr>
<tr><td>Mode 3: Anchor bolt failure</td><td colspan="3">$F_{\mathrm{T,3,Rd}} = 2F_{\mathrm{t,Rd}}$</td></tr>
<tr><td>Tensile resistance</td><td colspan="2">$F_{\mathrm{T,Rd}} = \min\left(F_{\mathrm{T,1,Rd}}, F_{\mathrm{T,2-1,Rd}}, F_{\mathrm{T,2,Rd}}, F_{\mathrm{T,3,Rd}}\right)$</td><td>$F_{\mathrm{T,Rd}} = \min\left(F_{\mathrm{T,1-2,Rd}}, F_{\mathrm{T,3,Rd}}\right)$</td></tr>
<tr><td colspan="4">$M_{\mathrm{pl,1,Rd}} = \dfrac{l_{\mathrm{eff,1}}t_{\mathrm{p}}^{2} f_{\mathrm{y}}}{4\gamma_{\mathrm{M0}}}$ $M_{\mathrm{pl,2,Rd}} = \dfrac{l_{\mathrm{eff,2}}t_{\mathrm{p}}^{2} f_{\mathrm{y}}}{4\gamma_{\mathrm{M0}}}$ $l_{\mathrm{eff,1}} = \min\left\{l_{\mathrm{eff,cp}}, l_{\mathrm{eff,1,nc}}\right\}$ $l_{\mathrm{eff,1,A,nc}} = \dfrac{\pi}{4}e_{\mathrm{x}}$, $l_{\mathrm{eff,1,bp}} = \dfrac{\pi}{4}d_{\mathrm{bp}}$, $l_{\mathrm{eff,1,C,nc}} = \dfrac{\pi}{4}\left(m_{\mathrm{x}} + e_{\mathrm{x}}\right)$
$M_{\mathrm{pl,1,A,Rd}} = \dfrac{l_{\mathrm{eff,1,A}}t_{\mathrm{p}}^{2} f_{\mathrm{y}}}{4\gamma_{\mathrm{M0}}}$ $M_{\mathrm{bp,1,Rd}} = \dfrac{l_{\mathrm{eff,1,bp}}t_{\mathrm{bp}}^{2} f_{\mathrm{y,bp}}}{4\gamma_{\mathrm{M0}}}$ $l_{\mathrm{eff,1,A}} = \min\left\{l_{\mathrm{eff,cp}}, l_{\mathrm{eff,1,A,nc}}\right\}$ $l_{\mathrm{eff,2-1,A,nc}} = \dfrac{\pi}{2}\left(e_{\mathrm{x}} - \xi_{\mathrm{T,2-1}}\right)$, $l_{\mathrm{eff,2-1,bp}} = \dfrac{\pi}{2}\left(\dfrac{d_{\mathrm{bp}}}{2} - \xi_{\mathrm{T,2-1}}\right)$
$M_{\mathrm{pl,1-2,Rd}} = \dfrac{l_{\mathrm{eff,1-2}}t_{\mathrm{p}}^{2} f_{\mathrm{y}}}{4\gamma_{\mathrm{M0}}}$ $l_{\mathrm{eff,cp}} = 2\pi m_{x}$ $l_{\mathrm{eff,2-1,C,nc}} = \dfrac{\pi}{2}\left(m_{\mathrm{x}} + e_{\mathrm{x}}\right)$
$M_{\mathrm{pl,2-1,Rd}} = \dfrac{l_{\mathrm{eff,2-1}}t_{\mathrm{p}}^{2} f_{\mathrm{y}}}{4\gamma_{\mathrm{M0}}}$ $M_{\mathrm{bp,2-1,Rd}} = \dfrac{l_{\mathrm{eff,2-1,bp}}t_{\mathrm{bp}}^{2} f_{\mathrm{y,bp}}}{4\gamma_{\mathrm{M0}}}$ $l_{\mathrm{eff,1,nc}} = l_{\mathrm{eff,1,A,nc}} + l_{\mathrm{eff,1,C,nc}}$ $n_{\mathrm{x,1}} = \min\left\{e_{\mathrm{x}}, 1.25m_{\mathrm{x}}\right\}$, $n_{\mathrm{x,2}} = \dfrac{e_{\mathrm{x}} + \xi_{\mathrm{T,2}}}{2}$
$l_{\mathrm{eff,1-2}} = l_{\mathrm{eff,1-2,nc}} = l_{\mathrm{eff,2-1,C,nc}}$
$l_{\mathrm{eff,2-1}} = l_{\mathrm{eff,2-1,nc}} = l_{\mathrm{eff,2-1,A,nc}} + l_{\mathrm{eff,2-1,C,nc}}$ $e_{\mathrm{w}} = \dfrac{d_{\mathrm{w}}}{4}$, $e_{\mathrm{bp}} = \dfrac{d_{\mathrm{bp}}}{4}$, $\gamma_{\mathrm{M0}} = 1$
$l_{\mathrm{eff,2}} = l_{\mathrm{eff,2,nc}} = l_{\mathrm{eff,2-1,C,nc}}$</td></tr>
<tr><td colspan="4">Method 2 assumes the anchor bolt force is uniformly distributed under the washer rather than concentrated along the bolt axis, which can help optimize the stub's strength.</td></tr>
</table>

$\xi_{\mathrm{T,2}}$ is obtained by solving the cubic equation:

$$\bar{X}^{3} - 2\alpha_{R}\bar{X}^{2} + \beta_{R} = 0 \text{ such that } \xi_{\mathrm{T,2}} = e_{\mathrm{x}}\left(1 - \bar{X}\right) \tag{5}$$

Where:

$$\alpha_R = \frac{e_x + m_x}{e_x} \text{ and } \beta_R = \frac{8(F_{t,Rd} m_x - M_{pl,C})}{\pi e_x^{\,3} f_{jd}}$$

The only real solution to the cubic equation is given by:

$$\bar{X} = \frac{1}{3}\left(\phi_R + \frac{4}{\phi_R} + 2\alpha_R\right) \Big| \beta_R \le 0 \text{ or } \beta_R \ge \frac{32\alpha_R^{\,3}}{27} \tag{6}$$

Where: $\phi_R = \sqrt[3]{\frac{3\sqrt{3}\sqrt{27\beta_R^{\,2} - 32\alpha_R^{\,3}\beta_R} + 16\alpha_R^{\,3} - 27\beta_R}{2}}$

Table 1 provides the tensile resistance considering the different failure modes and the useful effective lengths.

RESISTANCE OF THE COMPRESSIVE AREA

In the compressed zone, failure is determined by concrete compression and end-plate yielding, assessed using a compressed L-stub model as shown in Figure 7.

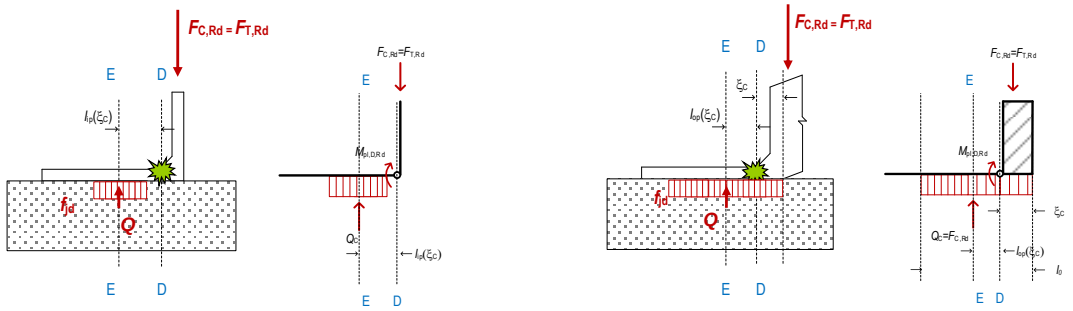

a) b)

Figure 7. Failure modes of L-stubs in compression a) In-plane bending b) Out-of-plane bending

The model calculates compressive resistance based on the localized concrete bearing strength, distributed over an effective area beneath the flange. Equilibrium is maintained by balancing this resistance with the tensile one, with the primary unknown being the distance *DE*, defined as the distance from the weld root to the centre of compression, $l(\xi_C)$, as specified in Equation (7). For in-plane bending, concrete beneath the beam flange is not compressed, while out-of-plane bending introduces compression, which the model addresses. The localized concrete bearing strength, f_{jd}, is conservatively taken as three times its design compressive strength, f_{cd}. The effective length of the yield line, $b_{eff,C,}$ depends on the bending orientation, adjusting for flange width or thickness by the additional bearing width, c.

$$l_{ip}(\xi_C) = \frac{M_{pl,D}}{F_{T,Rd}} \text{ and } l_{op}(\xi_C) = \frac{F_{T,Rd}}{2 f_{jd} b_{eff,C,op}} - \xi_C \tag{7}$$

Where,

$$M_{\mathrm{pl,D}} = \frac{b_{\mathrm{eff,C}} t_{\mathrm{p}}^2 f_{\mathrm{y}}}{4},\ \xi_{\mathrm{C}} = \frac{F_{\mathrm{T,Rd}} - \sqrt{2 M_{\mathrm{pl,D}} f_{\mathrm{jd}} b_{\mathrm{eff,C,op}}}}{f_{\mathrm{jd}} b_{\mathrm{eff,C,op}}} \geq 0,\ b_{\mathrm{eff,C}} = \begin{cases} b_{\mathrm{eff,C,ip}} = b_{\mathrm{c}} + 2c \\ b_{\mathrm{eff,C,op}} = 2\left(t_{\mathrm{f}} + 2c\right) \end{cases},\quad c = t_{\mathrm{p}} \sqrt{\frac{f_{\mathrm{y}}}{2 f_{\mathrm{jd}} \gamma_{\mathrm{M0}}}}$$

BENDING RESISTANCE

The in-plane and out-of-plane bending resistances, M_{Rd}, are calculated using Equation (8):

$$M_{\mathrm{Rd}} = F_{\mathrm{T,Rd}} \left(z_{\mathrm{T}} + z_{\mathrm{C}} \right) \tag{8}$$

The lever arms z_{T} and z_{C} are the distances from the beam centroid to the point of application of the tensile and compressive forces:

$$\begin{aligned} z_{\mathrm{T,ip}} &= \frac{h_{\mathrm{c}}}{2} + 0.8 a_{\mathrm{f}} + m_{\mathrm{x}} \frac{\sqrt{2}}{2},\ z_{\mathrm{T,op}} = \frac{b_{\mathrm{c}}}{2} + 0.8 a_{\mathrm{f}} + m_{\mathrm{x}} \frac{\sqrt{2}}{2} \\ z_{\mathrm{C,ip}} &= \frac{h_{\mathrm{c}}}{2} + 0.8 a_{\mathrm{f}} \sqrt{2} + l_{\mathrm{ip}} \left(\xi_{\mathrm{C}} \right),\ z_{\mathrm{C,op}} = \frac{b_{\mathrm{c}}}{2} + 0.8 a_{\mathrm{f}} \sqrt{2} + l_{\mathrm{op}} \left(\xi_{\mathrm{C}} \right) \end{aligned} \tag{9}$$

For biaxial bending moment, an elliptical interaction curve is considered. This approach has been validated by previous experimental studies performed by Seco et al. (2021) and Sonna Donko et al. (2024, 2025), and is also incorporated in the third edition of AISC Design Guide 1 (2024).

COMPARISON WITH EXPERIMENTAL TEST RESULTS

The proposed analytical method has been compared against experimental data from 12 tests performed by the authors (2025). The elastic approach of Lescouarc'h with Delesques' effective lengths, used through RCC-M, and the AISC DG1 method are also applied. The tested connections comprised an HEB 200 beam of S355 steel welded to a 400 × 400 mm end-plate of S275 steel using a nominal 9 mm fillet weld. These assemblies were anchored to a 770 × 900 × 1450 mm reinforced concrete block with four M22 class 4.6 anchor bolts. End-plates were tested for three thicknesses: 10, 15, and 20 mm (TP10/15/20)—under in-plane bending (M0), out-of-plane bending (M90), and biaxial bending at 30° and 45° (M30 and M45). Key geometric and material properties used in the computations are shown in Figure 8 and Table 2 respectively, including Packer et al.'s (1989) maximum stress, f_{p}.

For comparison with experimental results, mean material properties are used and safety/resistance factors are set to 1 in analytical models. Packer et al.'s maximum stress is applied to calculate resistances under Mode 1, where full end-plate yielding dominates. For design applications, nominal yield strength values should be adopted. Table 3 shows that the proposed method demonstrates the closest alignment with experimental results, showing a maximum deviation of 9.9% but on the safe side. In contrast, the elastic method significantly underestimates the connection strength, with deviations ranging from 51.0% to 83.9%, primarily due to its limited elastic stress range that restricts force redistribution in the end-plate and anchor bolts. Under biaxial bending, the elastic method's linear force distribution also fails to fully utilize anchor bolt capacity. The AISC DG1 method shows better accuracy than the elastic method but still underestimates strength for thin end-plates and out-of-plane bending moments, with discrepancies, reaching 54.7%. This

underestimation is attributed to assumptions regarding yield lines parallel to the flanges and incomplete utilization of anchor bolt capacity limited by end-plate failure in the tensile area.

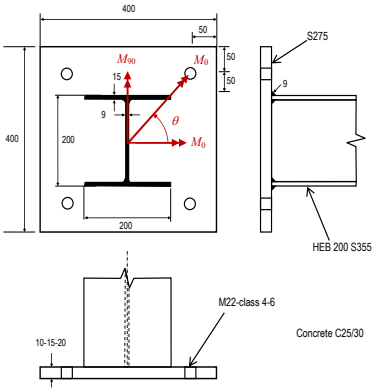

Figure 8. Geometric properties of the connection

Table 2 : Material properties of steel components

Component	E	f_y	f_u	f_p
	GPa	N/mm²	N/mm²	N/mm²
TP10-M0/30/45/90	212.6	407.4	501.0	469.8
TP15-M0/30	236.0	499.7	564.2	542.7
TP15-M45/90	236.4	367.5	527.1	473.9
TP20-M0/30/45/90	209.9	342.0	508.4	452.9
Anchor bolt	200.5	534.6	682.6	633.3

Table 3 : Comparison between analytical and experimental results

Specimen	t_p	f_{cm}	Ultimate bending moment				Deviation from test results		
			Test	Elastic Method	AISC DG1	Proposed	Elastic Method	AISC DG1	Proposed
	mm	N/mm²	kNm	kNm	kNm	kNm	%	%	%
TP10-M0	9.8	27.86	51.7	13.5	29.7	54.1	74.0	42.5	4.6
TP10-M30	10.1	26.96	54.9	11.1	27.7	53.8	79.8	49.6	2.1
TP10-M45	10.0	38.93	57.4	9.3	26.0	53.4	83.9	54.7	6.9
TP10-M90	10.0	28.65	50.5	13.5	23.4	52.8	73.3	53.7	4.5
TP15-M0	16.1	25.03	87.5	37.1	81.3	85.4	57.6	7.0	2.4
TP15-M30	16.1	25.01	85.7	30.6	75.8	81.0	64.3	11.6	5.5
TP15-M45	15.0	38.45	76.7	18.7	45.6	69.7	75.6	40.5	9.1
TP15-M90	15.0	28.43	66.3	27.3	41.1	68.7	58.8	38.1	3.6
TP20-M0	20.1	32.34	93.5	45.2	85.8	87.1	51.7	8.2	6.8
TP20-M30	20.0	32.83	93.4	37.2	80.0	86.2	60.2	14.4	7.7
TP20-M45	20.0	29.15	88.9	31.0	75.1	85.2	65.1	15.5	4.2
TP20-M90	20.0	31.79	92.3	45.2	67.6	83.2	51.0	26.7	9.9

The results of AISC DG1 are improved in presence of thicker plates. Overall, the proposed method, leveraging experimental insights and addressing limitations in the other methods, provided the most accurate predictions of connection strength across different end-plate thicknesses and bending moment orientations.

CONCLUSION

The present study evaluates the bending resistance of corner-bolted steel-to-concrete end-plate connections, highlighting gaps between an elastic approach through RCC-M, Eurocode 3, and AISC DG1 design methods. A new analytical model based on limit analysis and an elliptical interaction curve is proposed and validated against 12 experimental tests, showing a maximum deviation lower than 9.9% (but on the safe side). This model improves accuracy by incorporating key insights such as realistic yield line patterns and surface contact area. It challenges conservative assumptions in current codes, demonstrating the significant impact of anchor bolt placement and end-plate thickness on force distribution and strength. The findings advocate for revisions in existing design codes to better capture the actual strength of such connections, especially in the nuclear sector.

REFERENCES

AFCEN. (2025). *RCC-M 2024: Design and Construction Rules for Mechanical Equipment of PWR Nuclear Islands (in french)*. Association Française pour les règles de conception, de construction et de surveillance en exploitation des matériels des Chaudières Electro-Nucléaires.

AISC. (2024). *Steel Design Guide 1 Third Edition—Base connection design for steel structures. American Institute of Steel Construction, Inc.* (3).

ASME. (1963). *ASME Boiler and Pressure Vessel Code, Section III: Rules for Construction of Nuclear Facility Components, Division 1*. American Society of Mechanical Engineers.

CEN. (2005). *EN 1993-1-8 (Eurocode 3): Design of steel structures—Part 1-8: Design of joints.*

Da Silva Seco, L., Couchaux, M., Hjiaj, M., & Neves, L. C. (2021). Column base-plates under biaxial bending moment. *Engineering Structures, 231,* 111386.

Delesques, R. (1971). Resistance of column end-plates (in French). *Revue Construction Métallique, 3,* 36–41.

Fasaee, M. A. K., Banan, M. R., & Ghazizadeh, S. (2018). Capacity of exposed column base connections subjected to uniaxial and biaxial bending moments. *Journal of Constructional Steel Research, 148,* 361–370.

Kanvinde, A. M., Higgins, P., Cooke, R. J., Perez, J., & Higgins, J. (2015). Column Base Connections for Hollow Steel Sections: Seismic Performance and Strength Models. *Journal of Structural Engineering, 141*(7), 04014171.

Lescouarc'h, Y. (1988). *Rigid steel column bases (in French). Centre Technique Industriel de la Construction métallique.* Collection CTICM.

Packer, J. A., Bruno, L., & Birkemoe, P. C. (1989). Limit Analysis of Bolted RHS Flange Plate Joints. *Journal of Structural Engineering, 115*(9), 2226–2242.

Sonna Donko, M., Couchaux, M., & Boudot, J.-P. (2025, 03/09). *Experiments on steel-to-concrete corner-bolted end-plates under biaxial bending*. The 9th International Conference on Structural Engineering, Mechanics and Computation, Cape Town, South Africa.

Sonna Donko, M., Couchaux, M., Boudot, J.-P., & Boulle, N. (2024, 28/06). *Corner-bolted steel-to-concrete end-plate connections: Experimental and numerical investigations under biaxial bending*. The 15th Nordic Steel Construction Conference, Lulea, Sweden.